Published in final edited form as:
Neuron. 2014 August 6; 83(3): 558–571. doi:10.1016/j.neuron.2014.06.022.

Loss of *Dishevelled*s disrupts planar polarity in ependymal motile cilia and results in hydrocephalus

Shinya Ohata[1,*], **Jin Nakatani**[2,3,*], **Vicente Herranz-Pérez**[4,5], **JrGang Cheng**[6], **Haim Belinson**[2], **Toshiro Inubushi**[3], **William D. Snider**[6], **Jose Manuel García-Verdugo**[4,5], **Anthony Wynshaw-Boris**[2,7,†], and **Arturo Álvarez-Buylla**[1,†]

[1] Department of Neurological Surgery and Eli and Edythe Broad Center of Regeneration Medicine and Stem Cell Research, University of California, San Francisco (UCSF), San Francisco, CA 94143, USA

[2] Department of Pediatrics and Institute for Human Genetics, School of Medicine, UCSF, San Francisco, CA 94143, USA

[3] Biomedical MR Science Center, Shiga University of Medical Science, Ohtsu, Shiga 520-2192, Japan

[4] Laboratorio de Neurobiología Comparada, Instituto Cavanilles, Universidad de Valencia, CIBERNED, 46980 Valencia, Spain

[5] Unidad Mixta de Esclerosis Múltiple y Neurorregeneración, IIS Hospital La Fe, Valencia, Spain

[6] UNC Neuroscience Center, University of North Carolina, Chapel Hill, NC 27599, USA

[7] Department of Genetics and Genome Sciences, School of Medicine, Case Western Reserve University, Cleveland, OH 44106, USA

SUMMARY

Defects in ependymal (E) cells, which line the ventricle and generate cerebrospinal fluid flow through ciliary beating, can cause hydrocephalus. *Dishevelled* genes (*Dvl*s) are essential for Wnt signaling and Dvl2 has been shown to localize to the rootlet of motile cilia. Using the *hGFAP-Cre;Dvl1*$^{-/-}$*;2*$^{flox/flox}$*;3*$^{+/-}$ mouse, we show that compound genetic ablation of *Dvl*s causes hydrocephalus. In *hGFAP-Cre;Dvl1*$^{-/-}$*;2*$^{flox/flox}$*;3*$^{+/-}$ mutants, E cells differentiated normally, but the intracellular and intercellular rotational alignments of ependymal motile cilia were disrupted. As a consequence, the fluid flow generated by the *hGFAP-Cre;Dvl1*$^{-/-}$*;2*$^{flox/flox}$*;3*$^{+/-}$ E cells was significantly slower than that observed in control mice. *Dvl*s were also required for the proper

† Co-principal investigators and co-corresponding authors: Anthony Wynshaw-Boris, M. D., Ph. D. Department of Genetics and Genome Sciences, School of Medicine, Case Western Reserve University, 10900 Euclid Avenue, BRB731, Cleveland, Ohio 44106-4955 Phone: (216) 368-0581 Fax: (216) 368-3832 ajw168@case.edu. Arturo Álvarez-Buylla, Ph. D. Department of Neurological Surgery and Eli and Edythe Broad Center of Regeneration Medicine and Stem Cell Research, UCSF, 35 Medical Center Way, Box 0525, San Francisco, CA 94143, USA Phone: (415) 514-2348 Fax: (415) 514-2346 ABuylla@stemcell.ucsf.edu.
*These authors contributed equally to this work

positioning of motile cilia on the apical surface. Tamoxifen-induced conditional removal of *Dvl*s in adult mice also resulted in defects in intracellular rotational alignment and positioning of ependymal motile cilia. These results suggest that *Dvl*s are continuously required for E cell planar polarity and may prevent hydrocephalus.

Keywords

Dishevelled; Ependymal Cells; Planar Cell Polarity; Cilia; Basal Body; Ventricle; Hydrocephalus; Wnt; Conditional Knockout Mouse

INTRODUCTION

Cerebrospinal fluid (CSF) continuously flows through the cerebral ventricular system and plays critical roles in the homeostasis of the brain (Miyan et al., 2003). Abnormal accumulation of CSF leads to expansion of the ventricles resulting in hydrocephalus or ventriculomegaly. Hydrocephalus is a severe neurological disorder with high mortality (Casey et al., 1997; Del Bigio, 2010; Miyan et al., 2003; Vogel et al., 2012). The identification of genetic factors involved in the pathogenesis of hydrocephalus is of high priority in developing genetic diagnosis and therapy.

Ependymal (E) cells are multiciliated epithelial cells that line the walls of the ventricles in the adult brain and generate directional CSF flow by beating their cilia (Del Bigio, 2010). Aberrant ciliogenesis and ciliary beating of the E cells can cause CSF accumulation and may result in hydrocephalus (Del Bigio, 2010; Lee, 2013; Matsuo et al., 2013; Mirzadeh et al., 2010b; Tissir and Goffinet, 2013; Tissir et al., 2010). Cilia are nucleated from microtubule-based basal bodies (BB). We have previously shown that E cells display two forms of planar cell polarity (PCP)(Mirzadeh et al., 2010b): 1) translational polarity, the asymmetric positioning of the cluster of BB (BB patch) on the apical surface of the E cell; 2) rotational polarity, the unidirectional orientation of individual BB within each E cell. In addition to the polarity within each E cell, there must be transcellular coordination of polarity to ensure coordinated ciliary beating within a sheet of epithelial cells. In the *Xenopus* larval skin and mouse trachea multiciliated cells, intercellular rotational polarity of BB (tissue-level polarity) has been demonstrated (Mitchell et al., 2009; Vladar et al., 2012; Wallingford, 2010). A similar mechanism probably exists in E cells to ensure proper tissue-level polarization. Although the well-coordinated stroke of motile cilia generating the unidirectional CSF flow is expected to depend on PCP in E cells (Bayly and Axelrod, 2011; Guirao et al., 2010; Hirota et al., 2010; Tissir and Goffinet, 2013; Wallingford, 2010), the mechanisms guiding, refining, and maintaining PCP of E cells remain unclear.

Wnt signaling regulates proliferation and planar polarization in multiple tissues (Gao, 2012; Gray et al., 2011; Herr et al., 2012; Wang et al., 2006; Wynshaw-Boris, 2012). Secreted Wnt ligand glycoproteins bind to their receptor, Frizzled (Fz), and then recruit the intracellular adaptor protein, the Dishevelled family of proteins (Dvl1, 2 and 3; hereafter collectively referred to as Dvls) to Fz. Downstream signaling of Dvls is classified into the canonical and non-canonical Wnt pathways. Activation of the canonical Wnt/β-catenin pathway results in the stabilization and nuclear translocalization of β-catenin to alter transcriptional activity of

target genes. By contrast, activation of the non-canonical Wnt/PCP pathway results in changes in epithelial polarity and tissue reorganization by modulating cytoskeletal organization and adhesion. Although Dvls are required for both the canonical and non-canonical Wnt pathways, its role in the nervous system *in vivo* has not been fully elucidated as *Dvl1*$^{-/-}$;*2*$^{-/-}$;*3*$^{-/-}$ mutant mice embryos die soon after implantation due to impaired gastrulation (Hashimoto et al., 2010).

In the present study, we generated a novel mutant mouse line that has a floxed *Dvl2* allele (*Dvl2*^{flox}). We show that the genetic ablation of five out of the six *Dvl*s in the brain in triple knockout mice (TKO) for *Dvl*s in *hGFAP-Cre;Dvl1*$^{-/-}$;*2*$^{flox/flox}$;*3*$^{+/-}$ (hereafter referred to as Dvl TKO$^{hGFAP\text{-}Cre}$) results in expansion of the ventricles and aberrant rotational and tissue-level polarity in E cells. The fluid flow generated by the mutant E cells was slower compared to control mice. In addition, we show that *Dvl*s are required for the refinement of the translational polarity during postnatal maturation in Dvl TKO$^{Nestin\text{-}Cre}$. Furthermore, analysis of tamoxifen inducible Dvl TKO$^{Nestin\text{-}CreER}$ revealed that *Dvl*s are involved in the maintenance of rotational and translational polarity in adult E cells. These results demonstrate that *Dvl*s are continually required for proper PCP of motile cilia in E cells and suggest that *Dvl*s may prevent hydrocephalus.

RESULTS

Ventricular expansion in Dvl TKO$^{hGFAP\text{-}Cre}$ mouse

To generate mice that contain a floxed allele for *Dvl2* (*Dvl2*^{flox}), two *loxP* sequences were inserted into intron 1 and exon 15 of *Dvl2* (Fig. S1A). *hGFAP-Cre* mice express the Cre recombinase in radial glial cells (RG), which are embryonic neural progenitor cells, as early as embryonic day 14.5 (E14.5)(Zhuo et al., 2001). We confirmed the Cre-mediated ablation of *Dvl2*^{flox} using *hGFAP-Cre;Dvl2*$^{flox/+}$ mice (Fig. S1B). *Dvl2*$^{flox/flox}$ and *hGFAP-Cre;Dvl2*$^{flox/flox}$ mice brains were first analyzed histologically using sequential hematoxylin and eosin (H&E) stained coronal sections. No obvious anatomical abnormalities (including the size of the ventricles) were observed in the brain of *hGFAP-Cre;Dvl2*$^{flox/flox}$ mice compared to that of *Dvl2*$^{flox/flox}$ mice (Fig. 1A-H). To avoid a potential compensation for the loss of *Dvl2* by *Dvl1* and *Dvl3*, we crossed *hGFAP-Cre;Dvl2*$^{flox/flox}$ mice with *Dvl1*$^{-/-}$;*3*$^{+/-}$ mice and generated *hGFAP-Cre;Dvl1*$^{-/-}$;*2*$^{flox/flox}$;*3*$^{+/-}$ mice (hereafter referred to as Dvl TKO$^{hGFAP\text{-}Cre}$). We used littermates without *hGFAP-Cre*, i.e. *Dvl1*$^{-/-}$;*2*$^{flox/flox}$;*3*$^{+/-}$, as control mice (hereafter referred to as control). Dvl TKO$^{hGFAP\text{-}Cre}$ mice were viable for, at least, 6 months. At P31, the body weights were similar between control (18.0 ± 1.0 g, mean ± SEM, n = 4) and Dvl TKO$^{hGFAP\text{-}Cre}$ (17.0 ± 1.3 g, n = 4, $p = 0.54$) mice. We found that the lateral and third ventricles (LV and 3V, respectively) were enlarged in Dvl TKO$^{hGFAP\text{-}Cre}$ brain (Fig. 1I-P). Measurements of the LV and 3V volumes in Dvl TKO$^{hGFAP\text{-}Cre}$ mice showed a clear expansion of these cavities, but not of the 4V (n = 3 for each genotype, Fig. 1Q). The size of the LV was enlarged only in Dvl TKO$^{hGFAP\text{-}Cre}$, and was similar between *Dvl2*$^{flox/flox}$, *hGFAP-Cre;Dvl2*$^{flox/flox}$, and control mice. In the 3V, the expansion of ventricular size was also observed in *Dvl1*$^{-/-}$;*2*$^{flox/flox}$;*3*$^{+/-}$ mice and further enhanced in Dvl TKO$^{hGFAP\text{-}Cre}$ mice. Congenital hydrocephalus is observed in newborn children (Lee, 2013; Miyan et al., 2003). Expansion of the ventricles was not observed in

Dvl TKO$^{hGFAP\text{-}Cre}$ mice at P2 (Fig. S1C), suggesting that these mice develop hydrocephalus postnatally. Interestingly, there were no obvious effects on the size of cortex, striatum, and other brain regions in Dvl TKO$^{hGFAP\text{-}Cre}$ mutants at the gross anatomical level (Fig. 1I-P).

Anatomical analysis of the Sylvian aqueduct, subcommissural organ and choroid plexus

Stenosis in the Sylvian aqueduct is frequently associated with congenital hydrocephalus (Casey et al., 1997; Huh et al., 2009). This was not the cause of hydrocephalus in Dvl TKO$^{hGFAP\text{-}Cre}$ mice, as the Sylvian aqueduct was expanded compared to controls (Fig. 2A-H). The subcommissural organ (SCO) is a secretory gland positioned immediately anterior to the Sylvian aqueduct underneath the posterior commissure (Huh et al., 2009). Secretion of glycoproteins by the SCO facilitates CSF flow. It has been reported that spontaneous *Wnt1* mutant mice develop SCO agenesis and hydrocephalus (Louvi and Wassef, 2000). However, in Dvl TKO$^{hGFAP\text{-}Cre}$ mice, the SCO had a similar size compared to controls (Fig. 2I-K, n = 3 for each genotype), but appeared stretched -- likely due to the dilation of the ventricles. The choroid plexus produces CSF and overproduction of CSF can cause hydrocephalus (Miyan et al., 2003). We therefore measured the size of choroid plexus and found that it was similar between control and Dvl TKO$^{hGFAP\text{-}Cre}$ mice (Fig. 2L-R, n = 3 for each genotype). The expression of choroid plexus proteins (the homeobox transcription factor orthodenticle homeobox 2 (Otx2) and type I transmembrane adhesion molecule E-Cadherin) was similar in the choroid plexi of Dvl TKO$^{hGFAP\text{-}Cre}$ and control mice (Fig. 2S,T). These results suggest that the choroid plexus develops normally in Dvl TKO$^{hGFAP\text{-}Cre}$ mice.

Normal differentiation of E cells in Dvl TKO$^{hGFAP\text{-}Cre}$ mouse

Defects in both the differentiation and ciliogenesis of E cells can cause hydrocephalus (Jacquet et al., 2009; Mirzadeh et al., 2010b; Tissir and Goffinet, 2013; Tissir et al., 2010; Vogel et al., 2012). In mice, E cells differentiate from RG after P2 (Spassky et al., 2005). As the development of hydrocephalus in Dvl TKO$^{hGFAP\text{-}Cre}$ mice was also after P2 (Fig. 1I-Q,S1C), we suspected that the hydrocephalus in Dvl TKO$^{hGFAP\text{-}Cre}$ mice may be caused by some defect in E cells. In control mice, immunoreactivity of Dvl2 in P31 E cells was observed primarily within the BB patch (dotted circles in Fig. 3A) with some punctate staining outside the BB patch. This staining is consistent with previous observations in the developing mouse E cells, and multiciliated cells in mouse trachea and frog epidermis (Hirota et al., 2010; Park et al., 2008; Vladar et al., 2012). Dvl2-immunoreactivity was absent in Dvl TKO$^{hGFAP\text{-}Cre}$ mice (Fig. 3B), indicating that Dvl2 is effectively ablated in the Dvl TKO$^{hGFAP\text{-}Cre}$ mutant E cells. In the Kupffer's vesicle of zebrafish, the canonical Wnt/β-catenin pathway directly upregulates the expression of ciliogenic forkhead transcriptional factor FoxJ1 (Caron et al., 2012), which is essential for the maturation of mouse E cells (Jacquet et al., 2009). However, in control and Dvl TKO$^{hGFAP\text{-}Cre}$ mice, we observed normal expression of FoxJ1 and S100β (a calcium binding protein also expressed in differentiated E cells)(white arrows in Fig. 3C,D). E cells have large apical surfaces and multiple BB and are GFAP negative, while B1 cells have small apical surfaces and a single BB and are GFAP positive. On the apical surface, E cells surround B1 cells (white arrows in Fig. 3E,F) forming rosettes or pinwheels (Mirzadeh et al., 2008). Using wholemount staining for GFAP, β-catenin (localized to intercellular junctions), and γ-tubulin (localized to BB), we observed that the pinwheel organization was preserved in Dvl TKO$^{hGFAP\text{-}Cre}$ mice

(Fig. 3E,F). This indicates that E cells are normally produced and populate the ventricular epithelium in animals deficient in five out of six alleles of *Dvl*s. Overexpression of a dominant negative Dvl mutant associated with non-canonical Wnt/PCP pathway in the zebrafish Kupffer's vesicle or knocking down of *Dvl1* & *3* in the epidermis of the *Xenopus* embryo resulted in the shortening and reduction of the number of cilia (Oishi et al., 2006; Park et al., 2008). We therefore tested whether cilia morphology and number was affected in Dvl TKO$^{hGFAP\text{-}Cre}$ mice. Acetylated tubulin staining of ependymal motile cilia in wholemounts of the lateral walls of the lateral ventricle demonstrated normal length of cilia in E cells at P31 in Dvl TKO$^{hGFAP\text{-}Cre}$ mice (Fig. 3G,H). The number of BB in E cells was similar between control (n = 28 E cells from 4 mice, Fig. 3E,I,S3A) and Dvl TKO$^{hGFAP\text{-}Cre}$ mice (n = 24 E cells from 3 mice, $p = 0.93$, Fig. 3F,I,S3B). These data suggest that the differentiation of E cells is largely normal in Dvl TKO$^{hGFAP\text{-}Cre}$ mice.

Reduced speed of ependymal flow in Dvl TKO$^{hGFAP\text{-}Cre}$ mice

The continuous beating of cilia on the apical surface of E cells generates unidirectional fluid flow, known as ependymal flow (Miyan et al., 2003). Defects in this beating can cause hydrocephalus (Matsuo et al., 2013; Tissir et al., 2010). The dynamics of ependymal flow can be visualized and quantified by placing polystyrene latex fluorescent microbeads on live preparations of the lateral wall of the lateral ventricle (Fig. 4A)(Mirzadeh et al., 2010a; Mirzadeh et al., 2010b; Sawamoto et al., 2006). When a small number of microbeads were placed just caudal to the point of adhesion (PA) in the lateral ventricles in control mice, a strong dorsal to ventral current was detected (arrow in Fig. 4A, and 4B upper row, Movie S1). The velocity was quantified by measuring the distance that fluorescent beads travel within a defined time. In wholemount preparations of Dvl TKO$^{hGFAP\text{-}Cre}$ mice, the overall directionality of this flow was similar to that in controls (Fig. 4B lower row, Movie S2), but the speed was significantly slower compared to controls (Fig. 4C, n = 57 beads on 4 control mice, n = 65 beads on 5 Dvl TKO$^{hGFAP\text{-}Cre}$ mice). These results suggest that Dvls are required for the normal circulation of CSF.

Normal ciliary beating frequency in Dvl TKO$^{hGFAP\text{-}Cre}$ mice

The glycosyl phosphatidylinositol-anchored sialoglycoprotein CD24 localizes to the motile cilia of E cells (Guirao et al., 2010). To monitor the ciliary beating frequency (CBF, strokes/sec), we labeled wholemount preparation of the lateral walls of the lateral ventricle with anti-CD24 antibody conjugated with Phycoerythrin (PE), and monitored cilia behavior (Fig. 5A, Movie S3,4). CBF in the control (n = 101 E cells from 6 wholemount preparations, 4 mice) and in the Dvl TKO$^{hGFAP\text{-}Cre}$ mice (n = 41 E cells from 2 wholemount preparations, 1 mouse) were not significantly different (Fig. 5B). These results suggested that the reduction in the speed of ependymal flow in Dvl TKO$^{hGFAP\text{-}Cre}$ mice was not due to defects in CBF.

Disturbed rotational and tissue-level polarity of E cells in Dvl TKO$^{hGFAP\text{-}Cre}$ mice

Unlike the control E cells that displayed well-organized straight parallel bundles of cilia, the cilia in Dvl TKO$^{hGFAP\text{-}Cre}$ mice were disorganized, having an "uncombed" appearance (Fig. 3G,H). A similar disorganization of E cell motile cilia has been reported for *Celsr2* & *3* double mutant mice which was attributed to a defect in their rotational alignment (Tissir et

al., 2010). Centrosomal protein 164 (CEP164) localizes to the distal appendages in primary cilia of cultured cells (Graser et al., 2007; Steere et al., 2012) while γ-tubulin localizes to the BB. We found that in E cells, CEP164 is asymmetrically localized to one side of the BB (Fig. 6A). This allowed vector quantification of the rotational polarity of individual BB using confocal microscopy. We drew a vector from the CEP164-positive distal appendage to the γ-tubulin-positive BB (white arrows in Fig. 6A,B). Deviation of the rotational angle, expressed as the circular standard deviation (CSD, drawn as error bar on the graph in Fig. 6C) from the main orientation of BB for each E cell, was significantly larger in the Dvl TKO$^{hGFAP\text{-}Cre}$ E cells (Fig. 6B,C; CSD = 45°; n = 2,337 BB from 73 E cells, 4 mice) than in the control E cells (Fig. 6A,C; CSD = 30°; n = 2,229 BB from 83 E cells, 5 mice; $p < 0.001$). A basal foot protrudes laterally from the BB and "points" in the direction of CSF flow (Guirao et al., 2010; Hirota et al., 2010; Mirzadeh et al., 2010b). Therefore, the rotational orientation of each BB can be addressed by examining the position of both of these structures. In order to confirm the defect in rotational polarity in Dvl TKO$^{hGFAP\text{-}Cre}$ mice, we used transmission electron microscopy (TEM) in control and Dvl TKO$^{hGFAP\text{-}Cre}$ mice. We drew vectors from the center of the BB to the tip of the basal foot (Fig. 6D-I). This independent analysis showed a significant increase in CSD in Dvl TKO$^{hGFAP\text{-}Cre}$ E cells (Fig. 6J; CSD = 42°; n = 1129 BB from 131 cells, 3 mice) comparing to that in control E cells (CSD = 23°; n = 873 BB from 97 cells, 5 mice; $p < 0.001$). These results indicate that *Dvl*s are required for the coalignment in rotational polarity of BB in E cells. On the other hand, rotational polarity was not significantly affected in E cells in *hGFAP-Cre;Dvl2*$^{flox/flox}$ mice compared to that in *Dvl2*$^{flox/flox}$ mice (Fig. S2), suggesting that ablation of *Dvl2* alone is not sufficient to affect rotational polarity in E cells. This result is consistent with the observation that the ventricular size was similar between *Dvl2*$^{flox/flox}$ and *hGFAP-Cre;Dvl2*$^{flox/flox}$ mice (Fig. 1A-H,Q).

BB rotation is not only highly aligned within cells but also between cells within the epithelium. This alignment is known as tissue-level polarity in frog epidermis and mouse trachea (Mitchell et al., 2009; Vladar et al., 2012; Wallingford, 2010). The orientation of individual BB to CEP164 was averaged for each E cell and this mean orientation (vector, white arrows in Fig. 6K,L) was compared for a field of about 300 cells within the same regions in the control and Dvl TKO$^{hGFAP\text{-}Cre}$ mutant. Similarly to frog epidermis and mouse trachea, we found that BB in neighboring ependymal cells were highly coaligned, indicating that E cells also display tissue-level polarity (Fig. 6K,M, CSD = 23°, n = 296 cells from 6 control mice) . However, this coalignment between E cells was significantly affected in Dvl TKO$^{hGFAP\text{-}Cre}$ mice (Fig. 6L,M, CSD = 39°, n = 294 cells from 5 mice, $p < 0.001$). These results demonstrate that Dvls contribute to intercellular rotational alignment of ependymal BB.

Dvl-dependent refinement of translational polarity in the E cells

To analyze the roles of *Dvl*s in translational polarity, we drew vectors from the centers of apical surfaces of E cells to the centers of BB patches (red arrow in Fig. 7A). We measured the BB patch angle and the displacement from the center of the apical surface. BB patch angle and displacement were similar between Dvl TKO$^{hGFAP\text{-}Cre}$ mice and controls (Fig. S3A-F). The *GFAP-Cre* transgenic mice express the Cre recombinase from around E14

(Zhuo et al., 2001). It was possible that *Dvl2* deletion at this stage was ineffective, because this is past the time when translational polarity is established in RG (Mirzadeh et al., 2010b). We therefore analyzed Dvl TKO$^{\text{Nestin-Cre}}$ mutant mice that express the Cre-recombinase from E9 (Tronche et al., 1999). Similarly to Dvl TKO$^{\text{hGFAP-Cre}}$ mice, we observed that rotational polarity was disrupted in Dvl TKO$^{\text{Nestin-Cre}}$ mutant mice (Fig. S3G-M). For translational polarity, no significant differences in BB displacement were observed between control (n = 216 E cells from 5 mice) and Dvl TKO$^{\text{Nestin-Cre}}$ mice (n = 201 E cells from 5 mice, Fig. 7B-E,G), but BB patch angle had a slight, but significantly wider distribution in Dvl TKO$^{\text{Nestin-Cre}}$ mice (Fig. 7F, CSD = 79°, n = 224 E cells from 5 mice) compare d to controls at P31 (CSD = 44°, n = 321 E cells from 5 mice, $p < 0.002$).

Translational polarity is first established in RG (Mirzadeh et al., 2010b) -- the progenitors of E cells (Spassky et al., 2005). BB angle is further refined during development (Mirzadeh et al., 2010b). To address whether Dvls function in the establishment of translational polarity before E cell differentiation, we investigated the BB angle and displacement in RG of control and Dvl TKO$^{\text{Nestin-Cre}}$ mice at P2. CSD of BB angle was similar between control (Fig. 7H,J,L; CSD = 94°; n = 422 cells from 4 mice) and Dvl TKO$^{\text{Nestin-Cre}}$ mice (Fig. 7I,K,L; CSD = 85°; n = 527 cells from 3 mice; $0.1 < p < 0.2$). In addition, BB displacements were unchanged between control (Fig. 7M, n = 372 cells from 4 mice) and Dvl TKO$^{\text{Nestin-Cre}}$ mice (n = 306 cells from 3 mice). These results indicate that translational polarity is not affected in the Dvl TKO$^{\text{Nestin-Cre}}$ RG. Altogether, these results suggest that removal of five out of six *Dvl* alleles had minor effects on translational polarity. The small effect observed in the Dvl TKO$^{\text{Nestin-Cre}}$ E cells BB patch angle is likely due to its refinement during the differentiation of RG into E cells between P2 and P31.

Dvls involvement in maintaining BB polarity in E cells

Dvls continue to be expressed next to the BB of fully differentiated E cells (Fig. 3A). It has been shown that adult E cells express Nestin (Doetsch et al., 1997; Kuo et al., 2006). *Nestin-CreER* mice express a tamoxifen-inducible Cre-recombinase under the *Nestin* enhancer and promoter (Lagace et al., 2007). To test the possibility that Dvls function in the maintenance of ependymal PCP, we injected tamoxifen daily for 5 consecutive days (initiating the first injection between P30-35) in both the control and Dvl TKO$^{\text{Nestin-CreER}}$ mice (Fig. 8A). Two weeks after tamoxifen treatment, immunoreactivity for Dvl2 was absent in Dvl TKO$^{\text{Nestin-CreER}}$ E cells, indicating that Dvl2 was effectively knocked out (Fig. 8B,C). BB patch angle was significantly more widely distributed in Dvl TKO$^{\text{Nestin-CreER}}$ mice (CSD = 79°, n = 224 cells from 4 mice) compar ed to that of control mice (CSD = 48°, n = 321 cells f rom 4 mice, $p < 0.001$, Fig. 8D-F). However, BB patch displacement was unchanged in control (n = 142 cells from 3 mice) and Dvl TKO$^{\text{Nestin-CreER}}$ mice (n = 220 cells from 4 mice, Fig. 8G). The intracellular rotational alignment of BB was also significantly affected in Dvl TKO$^{\text{Nestin-CreER}}$ mice (CSD = 42°, n = 1813 BB from 92 cells, 4 mice) comp ared to control mice (CSD = 25°; n = 1636 BB from 82 cells, 4 mice; $p < 0.001$; Fig. 8H-J). The size of the LV was significantly bigger in Dvl TKO$^{\text{Nestin-CreER}}$ mice compared to that of control mice (Fig. S4). In contrast, tissue-level polarity was not affected when comparing control (CSD = 26°, n = 92 cells from 4 mice) and Dvl TKO$^{\text{Nestin-CreER}}$ mice (CSD = 20°, n

= 82 cells from 4 mice; $0.2 < p < 0.5$, Fig. 8K-M). Altogether, these results suggest that *Dvl*s are involved in maintaining rotational polarity and the BB patch angle in adult E cells.

DISCUSSION

*Dvl*s have redundant and overlapping functions (Wynshaw-Boris, 2012). For example, both *Dvl2*$^{-/-}$ and *Dvl3*$^{-/-}$ mice die at birth with cardiac defects, and *Dvl2*$^{-/-}$*;3*$^{-/-}$ mice are early embryonic lethal due to severe gastrulation defects (Etheridge et al., 2008; Hamblet et al., 2002; Hashimoto et al., 2010). In order to study the function of *Dvl*s *in vivo* while avoiding functional redundancy and lethality, we generated a *Dvl2*^{flox} mouse that was crossed to mice deficient in both *Dvl1* alleles and one *Dvl3* allele (a conditional *Dvl3*$^{flox/flox}$ mice has not been produced). In the present study, we used *hGFAP-Cre* to delete *Dvl2* in neural progenitor cells from around E14. These *hGFAP-Cre;Dvl1*$^{-/-}$*;2*$^{flox/flox}$*;3*$^{+/-}$ mice (Dvl TKO$^{hGFAP\text{-}Cre}$) developed hydrocephalus, which we found was due to defects in CSF flow. Interestingly, E cells, which line the ventricle and play a key role in CSF circulation, express Dvl2 in the apical domain in close association to the motile cilia BB as previously demonstrated (Hirota et al., 2010). Furthermore, we found that E cell PCP, and in particular rotational polarity of individual BB, develops abnormally in the absence of 5 out of 6 *Dvl* alleles. This observation is consistent with previous reports showing disruption in rotational alignment of motile cilia using a dominant negative Dvl2 in E cells (Hirota et al., 2010), knockdown of *Dvl1* & *3* in the frog epidermis (Park et al., 2008), or knockdown of *Clytia hemisphaerica Dishevelled* (*CheDsh*) in the ectoderm of *Clytia* embryos (Momose et al., 2012). In addition, we demonstrated that E cells exhibit intercellular coordination of BB alignment (tissue-level polarity) and *Dvl*s are involved in this polarity. *Dvl*s were also involved in the refinement of BB patch angle during the maturation of E cells. Interestingly, we found that *Dvl*s were not only important for the normal development of PCP in E cell cilia, but also for the maintenance of this PCP in the adult E cells.

Roles of Dvls in tissue-level polarity

In the present study, we show that E cells display intercellular coordination of BB orientation or tissue-level polarity. Tissue-level polarity has been found in multiciliated cells in frog epidermis (Mitchell et al., 2009) and mouse respiratory tract (Vladar et al., 2012). This correlated alignment of BB at the tissue-level was affected in the Dvl TKO$^{hGFAP\text{-}Cre}$ E cells (Fig. 6K-M). We cannot exclude the possibility that the observed dealignment at the tissue-level (Fig 6M) in Dvl TKO$^{hGFAP\text{-}Cre}$ mice is due to the defects in BB rotational polarity observed in individual E cells (Fig 6C). In these mice, the difference in CSD between controls and mutants in rotational polarity [45° (mutant) − 30° (control) = 15°] was similar to that in tissue-level polarity [39° (mutant) − 23° (control) = 16°]. However, disruption of rotational polarity is not necessarily associated with tissue-level polarity defects; in our Dvl TKO$^{Nestin\text{-}CreER}$ mice, rotational polarity in individual E cells was significantly disrupted ($p < 0.001$), but tissue-level polarity was unaffected ($0.2 < p < 0.5$) (Fig. 8H-M). It remains unclear why tissue-level polarity was not disrupted in Dvl TKO$^{Nestin\text{-}CreER}$ mice. One possibility is that the two-week interval after tamoxifen injection was not long enough for tissue-level polarity to become disorganized. Another possibility is that in Dvl TKO$^{Nestin\text{-}CreER}$ mice, one allele of *Dvl3* is sufficient to maintain tissue-level

polarity. It is also possible that *Dvl*s are not involved in the maintenance of tissue-level polarity.

Refinement of translational polarity by Dvls

Translational polarity, the asymmetric positioning of BB on the apical surface, is first observed in RG as early as E16, and this asymmetric distribution of BB gets refined gradually during development as a subpopulation of these progenitors transform into E cells (Mirzadeh et al., 2010b). In the present study, we show that in Dvl TKO$^{\text{Nestin-Cre}}$ mice the BB patch angle was partially affected in E cells at P31. Interestingly, this defect was not observed in the Dvl TKO$^{\text{Nestin-Cre}}$ mutant RG at P2. We previously found that *Dvl1*$^{-/-}$*;2*$^{-/-}$*;3*$^{+/-}$ or *Dvl1*$^{-/-}$*;2*$^{+/-}$*;3*$^{-/-}$ embryos displayed early disruption in the posterior migration of BB in node cells, resulting in defective nodal flow and left-right asymmetry defects (Hashimoto et al., 2010). Our results suggest that *Dvl*s also function in the refinement of translational polarity during the differentiation and maturation of E cells from RG. It remains unclear whether *Dvl*s are uninvolved in the establishment of translational polarity in RG or whether the one copy of *Dvl3* was sufficient to orchestrate the early polarization in RG.

Although the Cre-recombinase expression begins at around E14, we did not observe translational polarity defects in the Dvl TKO$^{\text{hGFAP-Cre}}$ mutant E cells, while the earlier ablation of *Dvl2* by *Nestin-Cre* in Dvl TKO$^{\text{Nestin-Cre}}$ mutants did result in such defects. The genetic ablation of *Dvl2* by *hGFAP-Cre* might not be early enough to affect the refinement of BB patch angle. We have reported a similar developmental stage-dependent effect on the BB patch angle and displacement in *Nestin-Cre;kif3a*$^{flox/flox}$ and *hGFAP-Cre;kif3a*$^{flox/flox}$ mice that lack a subunit of kinesin motor essential for the ciliogenesis (Mirzadeh et al., 2010b).

A transplantation study in the *Xenopus* larval skin revealed that *Dvl*s function in a cell-autonomous manner to establish rotational and tissue-level polarity in multiciliated cells (Mitchell et al., 2009). However the cell-autonomy of *Dvl*s in translational polarity has not been studied in the *Xenopus* larval skin, as these multiciliated cells do not exhibit translational polarity; BB cover the entire apical surface of the cells (Mitchell et al., 2009; Wallingford, 2010). It will be interesting to generate genetic chimera of *Dvl*s by injecting a Cre-expressing virus or electroporating a plasmid vector encoding Cre into the *Dvl1*$^{-/-}$*;2*$^{flox/flox}$*;3*$^{+/-}$ mice and analyze the translational polarity in E cells to analyze the cell-autonomy of *Dvl*s in translational polarity.

During the maturation of multiciliated cells, newly generated BB in the cytoplasm translocate to the apical area (apical docking) depending on *Dvl*s in the *Xenopus* epidermis and *Celsr2* & *3* in the mouse E cells (Park et al., 2008; Tissir et al., 2010). However, the BB patch was observed normally on the apical surface of the E cells in Dvl TKO$^{\text{Nestin-Cre}}$ and Dvl TKO$^{\text{hGFAP-Cre}}$ mutant mice (Fig. 3E,F,7B,C,S3A,B), suggesting that the apical docking of BB is not affected in the mutant E cells.

Role of Dvls in the maintenance of PCP

In *Drosophila*, a number of factors functioning in the establishment of PCP such as *Drosophila Dishevelled* (*Dsh*) have been identified (Bayly and Axelrod, 2011). However, it remains unknown whether PCP genes also function in the maintenance of PCP *in vivo*, although a computational simulation study has predicted that the PCP proteins such as the Wnt receptor Fz and atypical cadherin Flamingo/Celsr maintain PCP (Le Garrec et al., 2006). In the present study, we took advantage of a tamoxifen-inducible CreER line (*Nestin-CreER*) and demonstrate that *Dvl*s were required for the maintenance of rotational polarity and BB patch angle in E cells. The disruption in rotational polarity may result in reduction in the speed of the ependymal flow and abnormal accumulation of CSF, leading to the expansion of the LV (Fig. S4). It remains unclear why BB patch angle was unaffected in Dvl TKO$^{hGFAP\text{-}Cre}$ mice at P31, even though Dvl2 was eliminated from their E cells. As our Dvl TKO$^{hGFAP\text{-}Cre}$ mice still have one copy of *Dvl3*, there may be a compensatory mechanism for the chronic reduction in the Dvls activity such as upregulation of *Dvl3* expression, but this compensation is insufficient during acute deletion of *Dvl2* in Dvl TKO$^{Nestin\text{-}CreER}$ mice.

How do Dvls regulate the ependymal PCP?

It remains unclear how Dvls regulate rotational and translational polarity. Motile cilia are connected to the apical actin network through the rootlet (Werner et al., 2011). In E cells, Dvl2 is concentrated in the BB patch (Fig. 3A). It has been suggested that Dvl2 localizes to the rootlet of E cell motile cilia (Hirota et al., 2010). Dvls can interact directly with actin (Capelluto et al., 2002). Therefore Dvls may link motile cilia to the actin network. In the present study, we demonstrated that Dvl TKO$^{hGFAP\text{-}Cre}$ mice develop hydrocephalus. Mutations in the *coiled-coil domain-containing 88C* (*CCDC88C*) gene that encodes the Dvl-associating protein with a high frequency of leucine residues protein (DAPLE) have been implicated in the human autosomal recessive congenital hydrocephalus (Drielsma et al., 2012; Ekici et al., 2010). The mouse Daple protein facilitates Wnt5a-mediated actin remodeling by enhancing the interaction between Dvl2 and atypical protein kinase C λ (aPKCλ) to activate the small GTPase Rac1 in migrating cultured cells (Ishida-Takagishi et al., 2012). The actin-based motor protein nonmuscle myosin II is required to establish translational polarity but not rotational polarity in the developing mouse E cells (Hirota et al., 2010). In the frog epidermis, the small GTPase RhoA that promotes actin remodeling is required to generate the unidirectional flow, suggesting that RhoA plays important roles in the establishment of rotational polarity (Park et al., 2008). Altogether, the Dvl2/Daple protein complex may regulate ependymal PCP by activating aPKC, Rac1, and RhoA, leading to reorganization of the actin cytoskeleton.

Gene dosage effect of *Dvl*s on the canonical and non-canonical Wnt pathways

With the exception of the above PCP defects, the differentiation of E cells was apparently normal in Dvl TKO$^{hGFAP\text{-}Cre}$ mice that lack 5 out of 6 alleles of *Dvl*s (one copy of *Dvl3* remained intact). This observation is surprising given the key role of Dvls in the canonical Wnt signaling pathway (Wynshaw-Boris, 2012). In the zebrafish Kupffer's vesicle, the canonical Wnt pathway directly upregulates the expression *FoxJ1*, a gene required for the differentiation of E cells (Caron et al., 2012; Jacquet et al., 2009). We found that FoxJ1

expression was unaffected in E cells in Dvl TKO$^{hGFAP\text{-}Cre}$ mice. The expression of the canonical Wnt pathway target gene *Axin2* in the lateral and medial walls of lateral ventricle were similar in Dvl TKO$^{hGFAP\text{-}Cre}$ (*hGFAP-Cre;Dvl1*$^{-/-}$*;2*$^{flox/flox}$*;3*$^{+/-}$) mice and controls (*Dvl1*$^{-/-}$*;2*$^{flox/flox}$*;3*$^{+/-}$, data not shown). These data suggest that one allele of *Dvl3* may be sufficient for canonical Wnt signaling, but not for the non-canonical Wnt/PCP pathway during E cell differentiation. This view is consistent with previous reports demonstrating that most of the phenotypes in single and double knockout mice for *Dvl*s result from defects in the non-canonical Wnt/PCP pathway, rather than the canonical Wnt pathway (Wynshaw-Boris, 2012). Furthermore, among the two Planarian (*Schmidtea mediterranea*) *Dvl*s, only Dvl2 is involved in the canonical Wnt pathway, while both Dvl1 and 2 convey non-canonical Wnt signaling (Almuedo-Castillo et al., 2011; Dillman et al., 2013).

Redundancy of *Dvl*s in E cell PCP

The mechanism by which multiciliated cells properly orient their tufts of cilia is a fundamental problem in biology and medicine, playing essential roles not only in the brain, but also in the trachea and oviduct (Marshall and Kintner, 2008). Our studies demonstrate how subtle changes in PCP in E cell can result in hydrocephalus and provides evidence for the role of Dvls in orienting individual cilia for effective generation of fluid flow. Surprisingly, in the LV, these effects were only evident when 5 of 6 *Dvl* alleles were ablated (Fig. 1,6,S2), suggesting that mechanisms to assure proper development of PCP polarity in E cells are robust and highly redundant. This is likely due to the critical nature of E cell polarity for the proper circulation of CSF.

Dvls localize to different subcellular compartments depending on cell-types. In mouse embryonic fibroblasts, endogenous Dvl1 localizes to the BB of primary cilia (Abdelhamed et al., 2013; Zilber et al., 2013). In mouse tracheal epithelial cells, green fluorescent protein-tagged Dvl1 and 3 localize asymmetrically on the apical surface, while endogenous Dvl2 is associated with the BB of motile cilia (Vladar et al., 2012). Similarly, Dvl1 and Dvl2 are found next to the BB of motile cilia in mouse E cells and multiciliated cells in the frog skin (Guirao et al., 2010; Hirota et al., 2010; Park et al., 2008). Our findings are consistent with this localization of Dvl2 (Fig. 3A), suggesting that this isoform may be key to rotational polarity. However, removal of Dvl2 alone did not result in hydrocephalus or significant rotational misalignment (Fig. 1,S2). It remains to be determined where Dvl3 localize to in E cells and how Dvl1 and Dvl3 function redundantly with Dvl2 in the regulation of E cell PCP.

EXPERIMENTAL PROCEDURES

Animals

All animal experiments were performed following the guidelines of the UCSF Laboratory Animal Care and Use Committee. A targeted embryonic stem (ES) cell line (E14 strain 129P2Ola) with *Dvl2*^{flox} was established as previously described (Bouvier and Cheng, 2009), and injected into C57BL/6 wild-type (WT) blastocysts to generate chimeras. The chimeric mice were crossed with C57BL/6 WT mice to obtain *Dvl2*$^{flox/+}$ mice. To remove the Neo cassette, *Dvl2*$^{flox/+}$ mice were crossed with FLPeR mouse (Farley et al., 2000) (The

Jackson Laboratory, 003946). PCR genotyping was performed using the *Dvl2*^{flox} C (5'-GGA TTT TTC AGA CCG AGC AGA TTG-3') and F (5'-GAT CCA AAC CTC AAA GTA CCA CTC C-3') primers located inside the intron 1 to detect the WT (337 bp) and floxed (441 bp) alleles of the *Dvl2* gene (Fig. S1A). Cre-mediated recombination was confirmed by PCR using the *Dvl2*^{flox} G (5'-TTC AGC CTG GTG CCC TTC ATA GTG - 3') and J (5'-AAA GGC AGC TAC ACA GTC CCC AAC -3') primers surrounding the *loxP* site in exon 15 (WT, 412 bp; floxed, 506 bp; Fig. S1A,B). PCR using the *Dvl2*^{flox} C and J primers generate 393 bp products after Cre-mediated recombination. *Dvl1*$^{-/-}$ (Lijam et al., 1997), *Dvl3*$^{+/-}$ (Etheridge et al., 2008), *hGFAP-Cre* (Zhuo et al., 2001), *Nestin-Cre* (Tronche et al., 1999), and *Nestin-CreER* (Lagace et al., 2007) mice were generated previously. To obtain control and *Dvl*s mutant mice, *Dvl1*$^{-/-}$*;2*$^{flox/flox}$*;3*$^{+/-}$ mice were mated with *hGFAP-Cre;Dvl1*$^{-/-}$*;2*$^{flox/flox}$*;3*$^{+/+}$, *Nestin-Cre;Dvl1*$^{-/-}$*;2*$^{flox/flox}$*;3*$^{+/+}$ or *Nestin-CreER;Dvl1*$^{-/-}$*;2*$^{flox/flox}$*;3*$^{+/+}$ mice. All animals were kept in a 129Sv/Ev background. Adult mice (P30-35) were treated with 5 mg/30 g body weight/day tamoxifen in corn oil for 5 consecutive days via oral gavage and were euthanized after 2 weeks.

Histology, immunohistochemistry, and TEM

Histological, immunohistochemical, and TEM analyses were performed as previously described (Doetsch et al., 1997; Mirzadeh et al., 2010a; Mirzadeh et al., 2010b). Details are given in the Supplemental Experimental Procedures.

Ependymal flow assay and high-speed live imaging of ciliary beating

Wholemounts of the lateral wall of the lateral ventricle were freshly dissected as described previously (Mirzadeh et al., 2010a). For the ependymal flow assay, a glass micropipette filled with fluorescent polystyrene latex microbeads (2 μm, Polysciences) attached to an MO-10 micromanipulator (NARISHIGE) was lowered onto the wholemount, where microbeads were deposited onto the ventricular surface. We recorded the movement of microbeads using a Leica MZFLIII fluorescent dissection microscope and Retiga 2000R high-speed digital camera (QImaging) plugged into OpenLab imaging software (Improvision) at 10 frames per second (fps).

For high-speed imaging of ciliary beating, the wholemount preparations were incubated with rat anti-CD24 antibody conjugated with PE (1:100, BD Pharmingenin 553262) in Neurobasal medium (Gibco) supplemented with B-27 serum-free supplement (Gibco), glutamine and antibiotics for 20 min at room temperature (RT, 20-22°C), rinsed with L-15 medium (Gibco), and placed in a glass bottomed dish (BD Falcon). 1-2% low melting point agarose (invitrogen) and Neurobasal medium with the supplements were placed on the wholemounts. Ciliary beating was recorded with 15 msec exposure time at 61 fps for 200 frames at RT using a Leica DMI600 B microscope, HCX PL APO 100x oil-immersion lens (NA 1.44, Leica), Rolera EM-C^2 high-speed camera (QImaging) and Metamorph software.

Statistics

All results shown in the bar graphs are expressed as mean ± SEM. The means of two experimental groups were compared with two-tailed Student's *t*-test using the Excel software (Microsoft). The distributions of vectorial angles were compared with Watson's U^2

test using the Oriana software (Kovach Computing Services). For the volumetric analysis, we performed analysis of variance and Tukey's multiple comparisons test using SPSS (IBM) and GraphPad Prism (GraphPad Software). Differences were considered significant at $p < 0.05$.

Supplementary Material

Refer to Web version on PubMed Central for supplementary material.

Acknowledgments

The authors thank Drs. A. Messing for providing *hGFAP-Cre* mouse, G. Schütz for *Nestin-Cre* mouse, A.J. Eisch for *Nestin-CreER* mouse, T. Stearns and Y.L. Lee for anti-CEP164 antibody, A. Kriegstein, P. McQuillen and M. Ramalho-Santos for making equipment available, C. Boutin, Y. Hirota, D. Konno, Z. Mirzadeh, M. Sawada, T. Stowe, and E.K. Vladar for technical advice, S. GonzÁlez-Granero, C. Guinto, J.R. Rodriguez, R. Romero, and J. Zhou for technical help, J.L. Elsbernd, M.F. Paredes and C.K. Tong for proofreading, and all other members of A.W.-B. and A.A.-B. lab members for useful discussion. This work was sponsored by grants from Japanese Society for Promotion of Science (JSPS, KAKENHI 24240071 to T.I.) and National Institutes of Health (NS045892 to the UNC Neuroscience Center, NS050968 to W.D.S, NS073159 to A.W.-B. and HD032116 & NS28478 to A.A.-B.). S.O. was supported by the Cell Science Research Foundation, Kanae Foundation for the Promotion of Medical Science, TOYOBO Biotechnology Foundation, and JSPS Postdoctoral Fellowship for Research Abroad. A.A.-B. holds the Heather and Melanie Muss Endowed Chair.

REFERENCES

Abdelhamed ZA, Wheway G, Szymanska K, Natarajan S, Toomes C, Inglehearn C, Johnson CA. Variable expressivity of ciliopathy neurological phenotypes that encompass Meckel-Gruber syndrome and Joubert syndrome is caused by complex de-regulated ciliogenesis, Shh and Wnt signalling defects. Hum Mol Genet. 2013; 22:1358–1372. [PubMed: 23283079]

Almuedo-Castillo M, Saló E, Adell T. Dishevelled is essential for neural connectivity and planar cell polarity in planarians. Proc Natl Acad Sci U S A. 2011; 108:2813–2818. [PubMed: 21282632]

Bayly R, Axelrod JD. Pointing in the right direction: new developments in the field of planar cell polarity. Nat Rev Genet. 2011; 12:385–391. [PubMed: 21502960]

Bouvier J, Cheng JG. Recombineering-based procedure for creating Cre/loxP conditional knockouts in the mouse. Curr Protoc Mol Biol. 2009 Chapter 23, Unit 23.13.

Capelluto DG, Kutateladze TG, Habas R, Finkielstein CV, He X, Overduin M. The DIX domain targets dishevelled to actin stress fibres and vesicular membranes. Nature. 2002; 419:726–729. [PubMed: 12384700]

Caron A, Xu X, Lin X. Wnt/β-catenin signaling directly regulates Foxj1 expression and ciliogenesis in zebrafish Kupffer's vesicle. Development. 2012; 139:514–524. [PubMed: 22190638]

Casey AT, Kimmings EJ, Kleinlugtebeld AD, Taylor WA, Harkness WF, Hayward RD. The long-term outlook for hydrocephalus in childhood. A ten-year cohort study of 155 patients. Pediatr Neurosurg. 1997; 27:63–70.

Del Bigio MR. Ependymal cells: biology and pathology. Acta Neuropathol. 2010; 119:55–73. [PubMed: 20024659]

Dillman AR, Minor PJ, Sternberg PW. Origin and evolution of dishevelled. G3 (Bethesda). 2013; 3:251–262. [PubMed: 23390601]

Doetsch F, García-Verdugo JM, Alvarez-Buylla A. Cellular composition and three-dimensional organization of the subventricular germinal zone in the adult mammalian brain. J Neurosci. 1997; 17:5046–5061. [PubMed: 9185542]

Drielsma A, Jalas C, Simonis N, Désir J, Simanovsky N, Pirson I, Elpeleg O, Abramowicz M, Edvardson S. Two novel CCDC88C mutations confirm the role of DAPLE in autosomal recessive congenital hydrocephalus. J Med Genet. 2012; 49:708–712. [PubMed: 23042809]

Ekici AB, Hilfinger D, Jatzwauk M, Thiel CT, Wenzel D, Lorenz I, Boltshauser E, Goecke TW, Staatz G, Morris-Rosendahl DJ, et al. Disturbed Wnt Signalling due to a Mutation in CCDC88C Causes an Autosomal Recessive Non-Syndromic Hydrocephalus with Medial Diverticulum. Mol Syndromol. 2010; 1:99–112. [PubMed: 21031079]

Etheridge SL, Ray S, Li S, Hamblet NS, Lijam N, Tsang M, Greer J, Kardos N, Wang J, Sussman DJ, et al. Murine dishevelled 3 functions in redundant pathways with dishevelled 1 and 2 in normal cardiac outflow tract, cochlea, and neural tube development. PLoS Genet. 2008; 4:e1000259. [PubMed: 19008950]

Farley FW, Soriano P, Steffen LS, Dymecki SM. Widespread recombinase expression using FLPeR (flipper) mice. Genesis. 2000; 28:106–110. [PubMed: 11105051]

Gao B. Wnt Regulation of Planar Cell Polarity (PCP). Curr Top Dev Biol. 2012; 101:263–295. [PubMed: 23140633]

Graser S, Stierhof YD, Lavoie SB, Gassner OS, Lamla S, Le Clech M, Nigg EA. Cep164, a novel centriole appendage protein required for primary cilium formation. J Cell Biol. 2007; 179:321–330. [PubMed: 17954613]

Gray RS, Roszko I, Solnica-Krezel L. Planar cell polarity: coordinating morphogenetic cell behaviors with embryonic polarity. Dev Cell. 2011; 21:120–133. [PubMed: 21763613]

Guirao B, Meunier A, Mortaud S, Aguilar A, Corsi JM, Strehl L, Hirota Y, Desoeuvre A, Boutin C, Han YG, et al. Coupling between hydrodynamic forces and planar cell polarity orients mammalian motile cilia. Nat Cell Biol. 2010; 12:341–350. [PubMed: 20305650]

Hamblet NS, Lijam N, Ruiz-Lozano P, Wang J, Yang Y, Luo Z, Mei L, Chien KR, Sussman DJ, Wynshaw-Boris A. Dishevelled 2 is essential for cardiac outflow tract development, somite segmentation and neural tube closure. Development. 2002; 129:5827–5838. [PubMed: 12421720]

Hashimoto M, Shinohara K, Wang J, Ikeuchi S, Yoshiba S, Meno C, Nonaka S, Takada S, Hatta K, Wynshaw-Boris A, Hamada H. Planar polarization of node cells determines the rotational axis of node cilia. Nat Cell Biol. 2010; 12:170–176. [PubMed: 20098415]

Herr P, Hausmann G, Basler K. WNT secretion and signalling in human disease. Trends Mol Med. 2012; 18:483–493. [PubMed: 22796206]

Hirota Y, Meunier A, Huang S, Shimozawa T, Yamada O, Kida YS, Inoue M, Ito T, Kato H, Sakaguchi M, et al. Planar polarity of multiciliated ependymal cells involves the anterior migration of basal bodies regulated by non-muscle myosin II. Development. 2010; 137:3037–3046. [PubMed: 20685736]

Huh MS, Todd MA, Picketts DJ. SCO-ping out the mechanisms underlying the etiology of hydrocephalus. Physiology (Bethesda). 2009; 24:117–126. [PubMed: 19364914]

Ishida-Takagishi M, Enomoto A, Asai N, Ushida K, Watanabe T, Hashimoto T, Kato T, Weng L, Matsumoto S, Asai M, et al. The Dishevelled-associating protein Daple controls the non-canonical Wnt/Rac pathway and cell motility. Nat Commun. 2012; 3:859. [PubMed: 22643886]

Jacquet BV, Salinas-Mondragon R, Liang H, Therit B, Buie JD, Dykstra M, Campbell K, Ostrowski LE, Brody SL, Ghashghaei HT. FoxJ1-dependent gene expression is required for differentiation of radial glia into ependymal cells and a subset of astrocytes in the postnatal brain. Development. 2009; 136:4021–4031. [PubMed: 19906869]

Kuo CT, Mirzadeh Z, Soriano-Navarro M, Rasin M, Wang D, Shen J, Sestan N, Garcia-Verdugo J, Alvarez-Buylla A, Jan LY, Jan YN. Postnatal deletion of Numb/Numblike reveals repair and remodeling capacity in the subventricular neurogenic niche. Cell. 2006; 127:1253–1264. [PubMed: 17174898]

Lagace DC, Whitman MC, Noonan MA, Ables JL, DeCarolis NA, Arguello AA, Donovan MH, Fischer SJ, Farnbauch LA, Beech RD, et al. Dynamic contribution of nestin-expressing stem cells to adult neurogenesis. J Neurosci. 2007; 27:12623–12629. [PubMed: 18003841]

Le Garrec JF, Lopez P, Kerszberg M. Establishment and maintenance of planar epithelial cell polarity by asymmetric cadherin bridges: a computer model. Dev Dyn. 2006; 235:235–246. [PubMed: 16258926]

Lee L. Riding the wave of ependymal cilia: Genetic susceptibility to hydrocephalus in primary ciliary dyskinesia. J Neurosci Res. 2013; 91:1117–1132. [PubMed: 23686703]

Lijam N, Paylor R, McDonald MP, Crawley JN, Deng CX, Herrup K, Stevens KE, Maccaferri G, McBain CJ, Sussman DJ, Wynshaw-Boris A. Social interaction and sensorimotor gating abnormalities in mice lacking Dvl1. Cell. 1997; 90:895–905. [PubMed: 9298901]

Louvi A, Wassef M. Ectopic engrailed 1 expression in the dorsal midline causes cell death, abnormal differentiation of circumventricular organs and errors in axonal pathfinding. Development. 2000; 127:4061–4071. [PubMed: 10952903]

Marshall WF, Kintner C. Cilia orientation and the fluid mechanics of development. Curr Opin Cell Biol. 2008; 20:48–52. [PubMed: 18194854]

Matsuo M, Shimada A, Koshida S, Saga Y, Takeda H. The establishment of rotational polarity in the airway and ependymal cilia: analysis with a novel cilium motility mutant mouse. Am J Physiol Lung Cell Mol Physiol. 2013

Mirzadeh Z, Doetsch F, Sawamoto K, Wichterle H, Alvarez-Buylla A. The subventricular zone en-face: wholemount staining and ependymal flow. J Vis Exp. 2010a

Mirzadeh Z, Han YG, Soriano-Navarro M, García-Verdugo JM, Alvarez-Buylla A. Cilia organize ependymal planar polarity. J Neurosci. 2010b; 30:2600–2610. [PubMed: 20164345]

Mirzadeh Z, Merkle FT, Soriano-Navarro M, Garcia-Verdugo JM, Alvarez-Buylla A. Neural stem cells confer unique pinwheel architecture to the ventricular surface in neurogenic regions of the adult brain. Cell Stem Cell. 2008; 3:265–278. [PubMed: 18786414]

Mitchell B, Stubbs JL, Huisman F, Taborek P, Yu C, Kintner C. The PCP pathway instructs the planar orientation of ciliated cells in the Xenopus larval skin. Curr Biol. 2009; 19:924–929. [PubMed: 19427216]

Miyan JA, Nabiyouni M, Zendah M. Development of the brain: a vital role for cerebrospinal fluid. Can J Physiol Pharmacol. 2003; 81:317–328. [PubMed: 12769224]

Momose T, Kraus Y, Houliston E. A conserved function for Strabismus in establishing planar cell polarity in the ciliated ectoderm during cnidarian larval development. Development. 2012; 139:4374–4382. [PubMed: 23095884]

Oishi I, Kawakami Y, Raya A, Callol-Massot C, Izpisúa Belmonte JC. Regulation of primary cilia formation and left-right patterning in zebrafish by a noncanonical Wnt signaling mediator, duboraya. Nat Genet. 2006; 38:1316–1322. [PubMed: 17013396]

Park TJ, Mitchell BJ, Abitua PB, Kintner C, Wallingford JB. Dishevelled controls apical docking and planar polarization of basal bodies in ciliated epithelial cells. Nat Genet. 2008; 40:871–879. [PubMed: 18552847]

Sawamoto K, Wichterle H, Gonzalez-Perez O, Cholfin JA, Yamada M, Spassky N, Murcia NS, Garcia-Verdugo JM, Marin O, Rubenstein JL, et al. New neurons follow the flow of cerebrospinal fluid in the adult brain. Science. 2006; 311:629–632. [PubMed: 16410488]

Spassky N, Merkle FT, Flames N, Tramontin AD, García-Verdugo JM, Alvarez-Buylla A. Adult ependymal cells are postmitotic and are derived from radial glial cells during embryogenesis. J Neurosci. 2005; 25:10–18. [PubMed: 15634762]

Steere N, Chae V, Burke M, Li FQ, Takemaru K, Kuriyama R. A Wnt/beta-catenin pathway antagonist Chibby binds Cenexin at the distal end of mother centrioles and functions in primary cilia formation. PLoS One. 2012; 7:e41077. [PubMed: 22911743]

Tissir F, Goffinet AM. Shaping the nervous system: role of the core planar cell polarity genes. Nat Rev Neurosci. 2013; 14:525–535. [PubMed: 23839596]

Tissir F, Qu Y, Montcouquiol M, Zhou L, Komatsu K, Shi D, Fujimori T, Labeau J, Tyteca D, Courtoy P, et al. Lack of cadherins Celsr2 and Celsr3 impairs ependymal ciliogenesis, leading to fatal hydrocephalus. Nat Neurosci. 2010; 13:700–707. [PubMed: 20473291]

Tronche F, Kellendonk C, Kretz O, Gass P, Anlag K, Orban PC, Bock R, Klein R, Schütz G. Disruption of the glucocorticoid receptor gene in the nervous system results in reduced anxiety. Nat Genet. 1999; 23:99–103. [PubMed: 10471508]

Vladar EK, Bayly RD, Sangoram AM, Scott MP, Axelrod JD. Microtubules enable the planar cell polarity of airway cilia. Curr Biol. 2012; 22:2203–2212. [PubMed: 23122850]

Vogel P, Read RW, Hansen GM, Payne BJ, Small D, Sands AT, Zambrowicz BP. Congenital hydrocephalus in genetically engineered mice. Vet Pathol. 2012; 49:166–181. [PubMed: 21746835]

Wallingford JB. Planar cell polarity signaling, cilia and polarized ciliary beating. Curr Opin Cell Biol. 2010; 22:597–604. [PubMed: 20817501]

Wang J, Hamblet NS, Mark S, Dickinson ME, Brinkman BC, Segil N, Fraser SE, Chen P, Wallingford JB, Wynshaw-Boris A. Dishevelled genes mediate a conserved mammalian PCP pathway to regulate convergent extension during neurulation. Development. 2006; 133:1767–1778. [PubMed: 16571627]

Werner ME, Hwang P, Huisman F, Taborek P, Yu CC, Mitchell BJ. Actin and microtubules drive differential aspects of planar cell polarity in multiciliated cells. J Cell Biol. 2011; 195:19–26. [PubMed: 21949415]

Wynshaw-Boris A. Dishevelled: in vivo roles of a multifunctional gene family during development. Curr Top Dev Biol. 2012; 101:213–235. [PubMed: 23140631]

Zhuo L, Theis M, Alvarez-Maya I, Brenner M, Willecke K, Messing A. hGFAP-cre transgenic mice for manipulation of glial and neuronal function in vivo. Genesis. 2001; 31:85–94. [PubMed: 11668683]

Zilber Y, Babayeva S, Seo JH, Liu JJ, Mootin S, Torban E. The PCP effector Fuzzy controls cilial assembly and signaling by recruiting Rab8 and Dishevelled to the primary cilium. Mol Biol Cell. 2013; 24:555–565. [PubMed: 23303251]

- Ablation of 5 out of 6 *Dishevelled* genes (*Dvl*s) in mice resulted in hydrocephalus
- *Dvl*s were required for intra- and intercellular rotational alignment of E cell cilia
- *Dvl*s were required for asymmetric positioning of E cell motile cilia
- *Dvl*s were required to maintain orientation and localization of E cell motile cilia

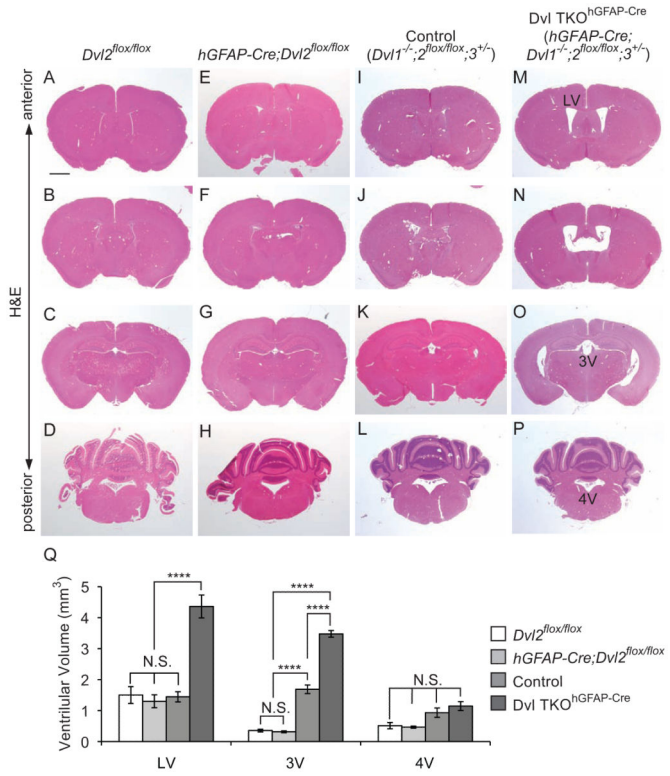

Figure 1. Enlarged ventricles in Dvl TKO$^{hGFAP\text{-}Cre}$ mice

(A-P) H&E staining of paraffin-embedded coronal sections of the *Dvl2$^{flox/flox}$* (A-D), *hGFAP-Cre;Dvl2$^{flox/flox}$* (E-H), control (I-L), and Dvl TKO$^{hGFAP\text{-}Cre}$ (M-P) mouse brains. Lateral (LV), third (3V), and fourth (4V) ventricles. Bar = 1 mm.

(Q) Volumetric analysis of the ventricles. Data shown are mean ± SEM. N.S., not significant; ****, $p < 0.001$.

See also Figure S1.

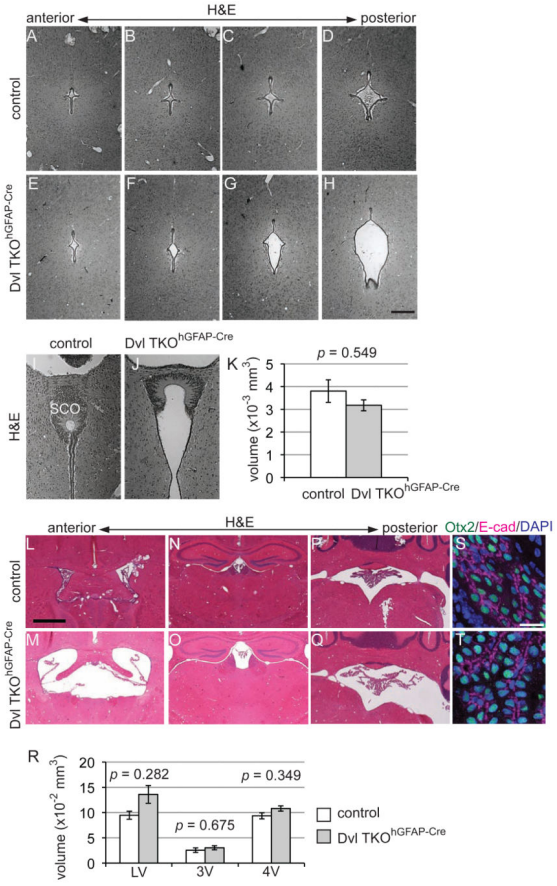

Figure 2. Anatomical analysis of the Sylvian aqueduct, subcommissural organ (SCO) and choroid plexus

(A-H) Coronal sections in the Sylvian aqueduct of control (A-D) and Dvl TKO$^{hGFAP\text{-}Cre}$ mutant (E-H) mice at P30 at 100 μm-interval from anterior (left) to posterior (right). Stenosis was not observed in any section in Dvl TKO$^{hGFAP\text{-}Cre}$. Bar = 250 μm.

(I,J) SCO structure of the control (I) and Dvl TKO$^{hGFAP\text{-}Cre}$ mutant (J) mice.

(K) Quantification of the volume of the SCO. The white and gray bars indicate control and Dvl TKO$^{hGFAP\text{-}Cre}$ mutant mice, respectively. Data shown are mean ± SEM.

(L-Q) Paraffin-embedded sections stained with H&E including the choroid plexus in LV (L,M), 3V (N,O) and 4V (P,Q) in the control (L,N,P) and Dvl TKO$^{hGFAP\text{-}Cre}$ (M,O,Q) mice are shown. Bar = 1 mm.

(R) Quantification of the volume of the choroid plexus in the control (white bars) and Dvl TKO$^{hGFAP\text{-}Cre}$ (gray bars) mice. Data shown are mean ± SEM.

(S,T) Immunohistochemical analysis of the choroid plexus. The control (S) and Dvl TKO$^{hGFAP\text{-}Cre}$ mutant (T) choroid plexus were stained with anti-Otx2 (green) and anti-E-cadherin (magenta) antibodies and DAPI (blue). Bar = 10 μm.

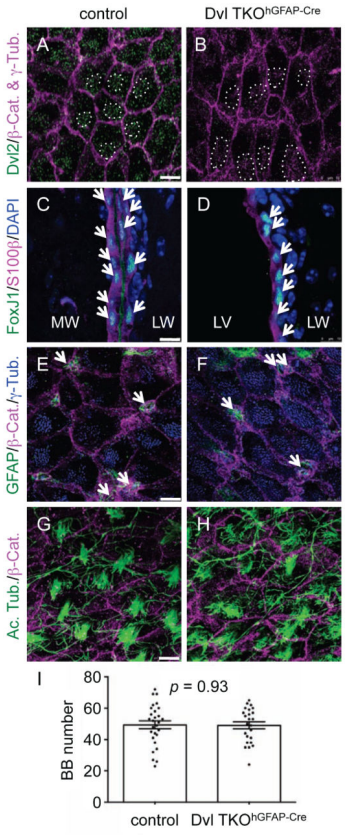

Figure 3. Differentiation of E cells was largely normal in Dvl TKO$^{hGFAP\text{-}Cre}$ mice

(A,B) Dvl2 localized to the BB patch in the control E cells, and was effectively knocked out in the Dvl TKO$^{hGFAP\text{-}Cre}$ E cells. Wholemount preparations of the lateral walls of lateral ventricle were stained with antibodies against Dvl2 (green), β-catenin & γ-tubulin (magenta) in control (A) and Dvl TKO$^{hGFAP\text{-}Cre}$ (B) mice. White dotted circles indicate the BB. Bar = 10 μm.

(C,D) The expression of E cell proteins was similar in control and Dvl TKO$^{hGFAP\text{-}Cre}$ mice. Coronal cryosections were stained with anti-FoxJ1 (green) and anti-S100β (magenta) antibodies and DAPI (blue) in control (C) and Dvl TKO$^{hGFAP\text{-}Cre}$ (D) mice. Bar = 10 μm. White arrows indicate FoxJ1 and S100β double-positive cells. Note that two layers of ependyma from the lateral and medial walls (LW and MW, respectively) of the lateral ventricles are shown in control (C), while only one layer from the lateral wall is shown in Dvl TKO$^{hGFAP\text{-}Cre}$ (D) due to the expansion of the lateral ventricle (LV) in Dvl TKO$^{hGFAP\text{-}Cre}$ mutant.

(E,F) The pinwheel organization of E cells surrounding B1 cells was preserved in Dvl TKO$^{hGFAP\text{-}Cre}$ mice. Wholemount preparations of the lateral walls of lateral ventricle were stained with antibodies against GFAP (green), β-catenin (magenta), and γ-tubulin (blue) in control (E) and Dvl TKO$^{hGFAP\text{-}Cre}$ (F) mice. White arrows indicate B1 cells at the center of pinwheel structures. Bar = 7.5 μm.

(G,H) Multiciliation of E cells was normal in Dvl TKO$^{hGFAP\text{-}Cre}$ mice. Wholemount preparations of the lateral walls of lateral ventricle were stained with antibodies against

acetylated tubulin (green, cilia) and β-catenin (magenta, intercellular junctions) in control (G) and Dvl TKO$^{hGFAP\text{-}Cre}$ (H) mice. Bar = 10 μm.

(I) The number of BB was similar in the control and Dvl TKO$^{hGFAP\text{-}Cre}$ E cells. Data shown are mean ± SEM. Each point on the graph is the number of BB in an individual E cell.

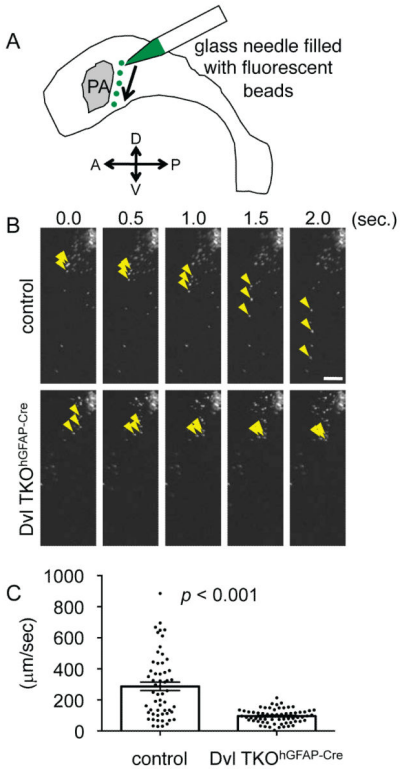

Figure 4. The speed of ependymal flow was significantly slower in Dvl TKO$^{hGFAP\text{-}Cre}$ mice

(A) Schematic of the ependymal flow assay. Fluorescent beads (green) were filled in a glass needle and placed onto wholemount preparations of the lateral walls of lateral ventricle. A, anterior; D, dorsal; P, posterior; PA, point of adhesion; V, ventral.

(B) Migration patterns of the fluorescent beads placed on the wholemount preparations of the lateral walls of lateral ventricle in control (upper row) and Dvl TKO$^{hGFAP\text{-}Cre}$ mutant (lower row). The yellow arrowheads indicate the position of three arbitrarily chosen fluorescent beads. Bar = 100 μm.

(C) The speed of fluorescent beads on the wholemount preparation was slower in Dvl TKO$^{hGFAP\text{-}Cre}$ mice. Data shown are mean ± SEM. Each point on the graph is speed of an individual fluorescent beads.

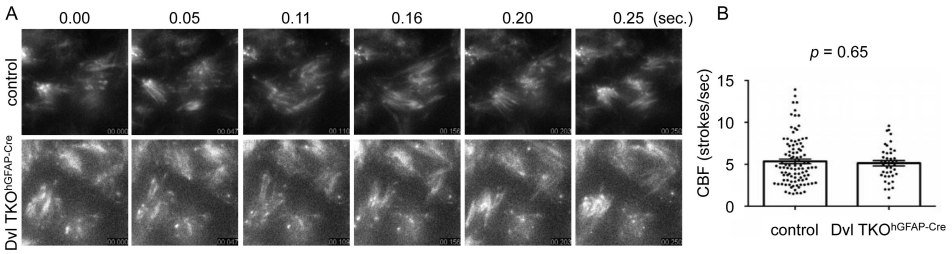

Figure 5. Ciliary beating frequency was unaffected in Dvl TKO$^{hGFAP\text{-}Cre}$ mice

(A) Sequential images of ciliary beating in control (upper row) and Dvl TKO$^{hGFAP\text{-}Cre}$ (lower row) mice.

(B) CBF in control and Dvl TKO$^{hGFAP\text{-}Cre}$ mice. Data shown are mean ± SEM. Each point on the graph is CBF of an individual E cell.

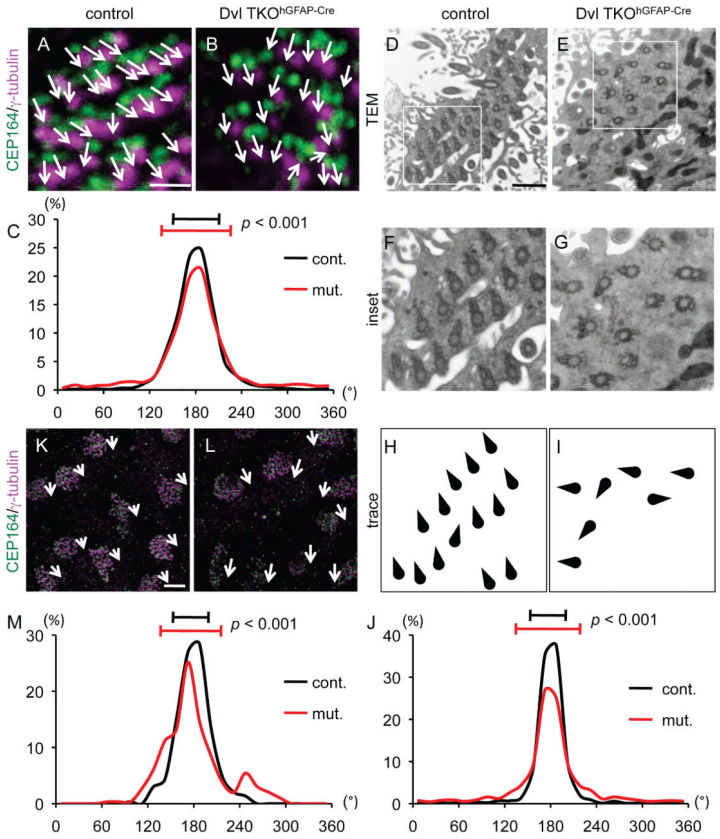

Figure 6. Rotational and tissue-level polarity were disrupted in the Dvl TKO$^{hGFAP\text{-}Cre}$ mutant E cells

(A,B) Wholemount preparations of the lateral walls of lateral ventricle were stained with antibodies against CEP164 (green) and γ-tubulin (magenta) in control (A) and Dvl TKO$^{hGFAP\text{-}Cre}$ (B) mice. White arrows indicate the direction of vectors. Bar = 1 μm.

(C) Histogram showing the distribution of the angle of vectors drawn from the center of CEP164-immunoreactivity to that of γ-tubulin in the control (cont., black) and Dvl TKO$^{hGFAP\text{-}Cre}$ (mut., red) E cells. Error bars on the graph show CSD.

(D-G) TEM analysis of rotational polarity in control (D,F) and Dvl TKO$^{hGFAP\text{-}Cre}$ (E,G) E cells. The region indicated in the white squares in D and E are magnified in F and G, respectively. Bar = 1 μm.

(H,I) Schematic drawings of BB shown in F and G illustrate the misalignment of BB rotational orientation.

(J) Histogram showing the distribution of the BB angle in the control (cont., black) and Dvl TKO$^{hGFAP\text{-}Cre}$ (mut., red) E cells. Error bars on the graph show CSD.

(K,L) Wholemount preparations of the lateral walls of lateral ventricle were stained with antibodies against CEP164 (green) and γ-tubulin (magenta) in control (K) and Dvl TKO$^{hGFAP\text{-}Cre}$ (L) mice. White arrows indicate the averaged angle of BB in each E cell. Bar = 5 μm.

(M) Histogram showing the distribution of the average angle of polarity vectors (white arrows in K,L) of E cell BB in control (cont, black) and Dvl TKO$^{hGFAP\text{-}Cre}$ (mut., red) mice. Error bars on the graph show CSD.

See also Figure S2.

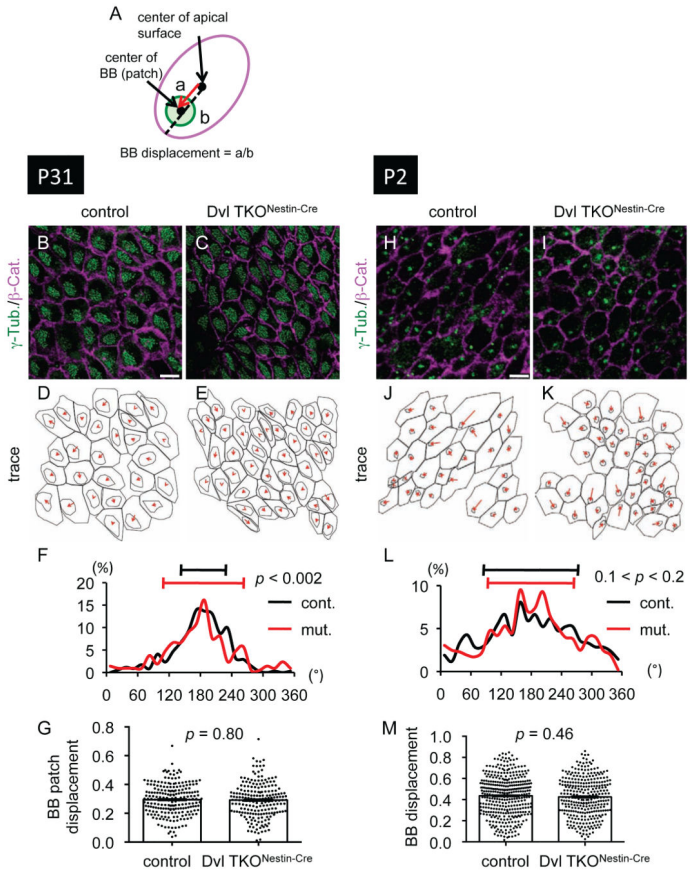

Figure 7. BB patch angle was disrupted in the Dvl TKO$^{Nestin\text{-}Cre}$ mutant E cells at P31

(A) Schematic drawing showing BB patch angle and BB patch displacement. Vectors (red arrow) were drawn from the center of apical surface to that of BB in RG or to that of BB patch in E cells. To calculate BB displacement, the length of the vector (a) was normalized with the length of the line extended to the edge of the apical surface (black dashed line, b). (B-M) Coordination of BB patch angle was affected in E cells at P31 but not in RG at P2 in Dvl TKO$^{Nestin\text{-}Cre}$ mice. (B,C,H,I) Wholemount preparations of the lateral walls of the lateral ventricle at P31 (B,C) and P2 (H,I) were stained with antibodies against γ-tubulin (green) and β-catenin (magenta) in control (B,H) and Dvl TKO$^{Nestin\text{-}Cre}$ (C,I) mice. Bars = 5 μm. (D,E,J,K) Traces of the intercellular junction labeled with β-catenin and BB labeled with γ-tubulin of E cells shown in B and C (D,E, respectively) and those of RG shown in H and I (J,K, respectively). The red arrows show the vectors drawn from the center of the apical surface to that of BB patch (D,E) or BB (J,K). (F,L) Histograms showing the distribution of the BB patch angles at P31 (F) and BB angles at P2 (L) in control (black) and Dvl TKO$^{Nestion\text{-}Cre}$ (red) mice. Error bars on the graph show CSD. (G,M) Quantification of BB patch displacement at P31 (G) and BB displacement at P2 (M). Data shown are mean ± SEM. Each point on the graphs is BB patch displacement of an individual E cell (G) and BB displacement of an individual RG (M).

See also Figure S3.

Figure 8. Dvl were required for the maintenance of coordination of BB patch angle and rotational polarity

(A) Timeline of the experiment used in the present study. Tamoxifen was given for 5 consequent days (red arrows) and the mice were sacrificed after 2 weeks (black arrow).

(B,C) Dvl2-immunoreactivity was significantly eliminated in Dvl TKO$^{Nestin\text{-}CreER}$ mice. Wholemount preparations of the lateral walls of lateral ventricle were stained with antibodies against Dvl2 (green), and β-catenin & γ-tubulin (magenta) in control (B) and Dvl TKO$^{Nestin\text{-}CreER}$ (C) mice. Bar = 20 μm.

(D-F) Dvls were required to maintain coordinated BB patch angle. (D,E) Wholemount preparations of the lateral walls of lateral ventricle were stained with antibodies against γ-tubulin (green) and β-catenin (magenta) in control (D) and Dvl TKO$^{Nestin\text{-}CreER}$ (E) mice. Bar = 20 μm. (F) Histogram showing the distribution of the BB patch angles in control (black) and Dvl TKO$^{Nestin\text{-}CreER}$ mutant (red) mice. Error bars on the graph show CSD.

(G) BB patch displacement was not affected in Dvl TKO$^{Nestin\text{-}CreER}$ mice in the present study. Data shown are mean ± SEM. Each point on the graph is BB patch displacement of an individual E cell.

(H-J) Dvls were required for the maintenance of rotational polarity. (H,I) Wholemount preparations of the lateral walls of lateral ventricle were stained with antibodies against CEP164 (green) and γ-tubulin (magenta) in control (H) and Dvl TKO$^{Nestin\text{-}CreER}$ (I) mice. Bar = 1 μm. (J) Histogram showing the distribution of the BB patch angles in control (black) and Dvl TKO$^{Nestin\text{-}CreER}$ (red) mice.

(K-M) Tissue-level polarity was not affected in Dvl TKO$^{Nestin\text{-}CreER}$ mice in the present study. (K,L) Wholemount preparations of the lateral walls of lateral ventricle were stained with antibodies against CEP164 (green) and γ-tubulin (magenta) in control (K) and Dvl TKO$^{Nestin\text{-}CreER}$ (L) mice. Bar = 5 μm. (M) Histogram showing the distribution of BB patch angles in control (black) and Dvl TKO$^{Nestin\text{-}CreER}$ (red) mice. Error bars on the graph show CSD.

See also Figure S4.